PUBLICATIONS OF THE ASTRONOMICAL SOCIETY OF THE PACIFIC, **118**:98–106, 2006 January

Spectral Energy Distributions of M81 Globular Clusters in the BATC Multicolor Survey

JUN MA,[1] XU ZHOU,[1] DAVID BURSTEIN,[2] JIANSHENG CHEN,[1] ZHAOJI JIANG,[1] ZHENYU WU,[1] AND JIANGHUA WU[1]
Received 2005 August 2; accepted 2005 September 26; published 2006 January 3

ABSTRACT. In this paper, we give the spectral energy distributions (SEDs) of 42 M81 globular clusters in 13 intermediate-band filters from 4000 to 10000 Å using the CCD images of M81, observed as part of the Beijing-Arizona-Taiwan-Connecticut (BATC) Multicolor Sky Survey. The BATC multicolor filter system is specifically designed to exclude most of the bright and variable night-sky emission lines, including the OH forest. Hence, it can present accurate SEDs of the observed objects. These SEDs are low-resolution spectra and can reflect the stellar populations of the globular clusters. This paper confirms the conclusions of Schroder et al., that M81 contains clusters as young as a few Gyr, which were also observed in both M31 and M33.

1. INTRODUCTION

The study of globular clusters (GCs) plays an important role in our understanding of the evolution and history of galaxies. They are bright and easily identifiable star clusters, typically with homogeneous abundances and ages. Galactic GCs, the stars of which are thought to be among the oldest stars in the universe, provide important information regarding the minimum age of the universe and the early formation history of our Galaxy. However, we also find that the GC system of our neighboring galaxy, M31, contains at least 20 young GCs, ranging in age from 100 Myr to ∼5 Gyr (Burstein et al. 2004; Beasley et al. 2005).

The galaxy M81 is one of the nearest large spirals outside the Local Group. As such, its globular cluster system has recently come under detailed scrutiny. Perelmuter & Racine (1995) first attempted to identify GCs in M81 from ground-based images, sifting through over 3700 objects in a 50′ diameter field centered on M81. They found 70 GC candidates within an 11 kpc galactocentric radius. Perelmuter et al. (1995) then confirmed 25 as M81 GCs, on the basis of spectroscopy of 82 bright GC candidates in the M81 field. Schroder et al. (2002) obtained moderate-resolution spectroscopy for 16 of the Perelmuter & Racine M81 GC candidates and found all of them to be GCs.

Recently, Chandar et al. (2001) discovered 114 compact star clusters in M81 from *B*-, *V*-, and *I*-band *Hubble Space Telescope* (*HST*) Wide Field Planetary Camera 2 images in eight fields, covering a total area of 40′; 54 of these are new GCs. Using these 95 M81 GCs, Ma et al. (2005) showed that the intrinsic *B* and *V* colors and metallicities of these GCs are bimodal, with metallicity peaks at [Fe/H] ≈ −1.45 and −0.53, similar to what we find for the Milky Way and M31 GCs. In this paper, we present new spectral energy distributions (SEDs) for 42 of these GCs, using M81 images observed as part of the galaxy calibration program of the Beijing-Arizona-Taiwan-Connecticut (BATC) Multicolor Sky Survey (e.g., Fan et al. 1996; Zheng et al. 1999). The BATC filters are a custom-designed set of 15 intermediate-band filters that were created to do spectrophotometry for preselected 1 deg^2 regions of the Northern sky.

Details of our observations and data reduction are given in § 2. Section 3 gives our summary.

2. OBSERVATIONS AND DATA REDUCTION

2.1. The Sample of GCs

Ma et al. (2005) studied the intrinsic *B* and *V* colors and metallicities of 95 M81 GCs. In order to study the stellar populations of these GCs, we extracted 311 images of the M81 field as part of the BATC multicolor survey of the sky, taken in 13 intermediate-band filters with a total exposure time of ∼100 hr from 1995 February 5 to 2002 April 30. Multiple images with the same filter were combined to improve the signal-to-noise ratio (S/N). While the SEDs of the sample GCs that are brighter than $V \sim 20$ mag can be obtained in the BATC multicolor system, we are constrained in obtaining full SEDs for these GCs by the limited field of view around M81, as well as by the location of some of these GCs in the high background of M81 itself. As such, we have obtained SEDs in 13 BATC filters for 42 of the 95 GCs that were previously presented.

2.2. Observations and Data Reduction

The BATC multicolor survey uses a Ford Aerospace 2048 × 2048 CCD camera with 15 μm pixels on the 0.6/0.9 m f/3 Schmidt telescope of the Xinglong Station of the National Astronomical Observatories, giving a CCD field of view of

[1] National Astronomical Observatories, Chinese Academy of Sciences, Beijing, 100012, China; majun@vega.bac.pku.edu.cn.

[2] Department of Physics and Astronomy, Box 871504, Arizona State University, Tempe, AZ 85287-1504.

TABLE 1
PARAMETERS OF THE BATC FILTERS, AND STATISTICS OF OBSERVATIONS FOR THE M81 FIELD

Number (1)	Name (2)	CW[a] (Å) (3)	Exposure (hr) (4)	N[b] (5)	rms[c] (6)
1	BATC03	4210	03:53	14	0.004
2	BATC04	4546	12:20	39	0.013
3	BATC05	4872	06:10	21	0.005
4	BATC06	5250	06:05	19	0.005
5	BATC07	5785	05:12	18	0.004
6	BATC08	6075	04:00	12	0.006
7	BATC09	6710	06:00	18	0.006
8	BATC10	7010	05:20	16	0.007
9	BATC11	7530	05:40	17	0.013
10	BATC12	8000	05:20	16	0.006
11	BATC13	8510	15:00	45	0.005
12	BATC14	9170	16:40	50	0.036
13	BATC15	9720	08:40	26	0.039

[a] Central wavelength for each BATC filter.
[b] Image numbers for each BATC filter.
[c] Calibration error, in magnitude, for each filter as obtained from the standard stars.

$58' \times 58'$, with a pixel size of 1.″7. The typical seeing at the Xinglong Station is 2″. The BATC multicolor filter system, which was specifically designed to avoid contamination from the brightest and most variable night-sky emission lines, includes 15 intermediate-band filters covering 3300 to 10000 Å. Calibrations of these images are made using observations of four F subdwarfs, HD 19445, HD 84937, BD +26 2606, and BD +17 4708, all taken from Oke & Gunn (1983). Therefore, our magnitudes are defined in a manner similar to the spectrophotometric AB magnitude system of Oke & Gunn, the $\tilde{f}_\nu$ monochromatic system. BATC magnitudes are defined on the AB magnitude system as

$$m_{\rm BATC} = -2.5 \log \tilde{F}_\nu - 48.60, \quad (1)$$

where $\tilde{F}_\nu$ is the appropriately averaged monochromatic flux in unit of ergs s^{-1} cm^{-2} Hz^{-1} at the effective wavelength of the specific passband. In the BATC system (Yan et al. 2000), $\tilde{F}_\nu$ is defined as

$$\tilde{F}_\nu = \frac{\int d(\log \nu)\, f_\nu\, r_\nu}{\int d(\log \nu)\, r_\nu}, \quad (2)$$

which links the magnitude to the number of photons detected by the CCD, rather than to the input flux (Fukugita et al. 1996). In equation (2), r_ν is the system's response, and f_ν is the SED of the source.

Of the 15 BATC filters available, we only used 13; we did not use the two bluest filters. Reduction of the CCD data proceeds with bias subtraction and flat-fielding with dome flats. These steps were performed with our custom-made, automatic data-reduction software PIPELINE I, developed for the BATC Multicolor Sky Survey (Fan et al. 1996; Zheng et al. 1999). The dome flat-field images were taken by using a diffuser plate in front of the correcting plate of the Schmidt telescope, a flat-fielding technique that has been verified with photometry we have done on other galaxies and fields of view (e.g., Fan et al. 1996; Zheng et al. 1999; Wu et al. 2002; Yan et al. 2000; Zhou et al. 2001, 2004). Spectrophotometric calibration of the M81 images using the Oke-Gunn standard stars is done during photometric nights (see details from Yan et al. 2000; Zhou et al. 2001).

Using the images of the standard stars observed on photometric nights, we iteratively derived the atmospheric extinction curves and the variation of these extinction coefficients with time (see, e.g., Yan et al. 2000; Zhou et al. 2001). The extinction coefficients at any given time in a night $[K + \Delta K(\rm UT)]$, and the zero points of the instrumental magnitudes (C), are obtained by

$$m_{\rm BATC} = m_{\rm inst} + [K + \Delta K(\rm UT)]X + C, \quad (3)$$

where X is the air mass. The instrumental magnitudes ($m_{\rm inst}$) of the selected bright, isolated, and unsaturated stars on the M81 field images of the same photometric nights can be readily transformed to the BATC AB magnitude system ($m_{\rm BATC}$). The calibrated magnitudes of these stars are obtained on the photometric nights, which are then used as secondary standards to uniformly combine images from calibrated nights with those taken during nonphotometric weather. Table 1 lists the parameters of the BATC multicolor filter system and the statistics of observations. Column (6) of Table 1 gives the scatter, in magnitudes, for the photometric observations of the four primary standard stars in each filter.

2.3. Integrated Photometry

For each M81 GC, the DAOPHOT routine PHOT (Stetson 1987) is used to obtain magnitudes. To avoid contamination from nearby objects, we adopt a small aperture of 6.″8, corresponding to a diameter of 4 pixels in the Ford CCD. Aperture corrections are determined as follows, using the isolated M81 GC Is40165. We determine the magnitude differences between photometric diameters of 4 and 10 pixels in each of the 13 BATC filters. Inner and outer radii of the sky apertures are from 4 to 7 pixels, for a diameter of 4 pixels, and from 6 to 10 pixels, for a diameter of 10 pixels, respectively. The SEDs obtained in this manner are given in Table 2. Column (1) lists the GC's name, taken from Perelmuter et al. (1995), Schroder et al. (2002), and Chandar et al. (2001). Columns (2) to (14) give the magnitudes of the 13 observed BATC passbands. The second row for each GC gives the 1 σ errors in magnitude for the corresponding passband. The errors for each filter are given by DAOPHOT. Magnitudes in the BATC03 filter could not be

TABLE 2
SEDs of 42 Globular Clusters in M81

Name (1)	BATC03 (4210 Å) (1)	BATC04 (4546 Å) (1)	BATC05 (4872 Å) (1)	BATC06 (5250 Å) (1)	BATC07 (5785 Å) (1)	BATC08 (6075 Å) (1)	BATC09 (6710 Å) (1)	BATC10 (7010 Å) (1)	BATC11 (7530 Å) (1)	BATC12 (8000 Å) (1)	BATC13 (8510 Å) (1)	BATC14 (9170 Å) (1)	BATC15 (9720 Å) (1)
Is40083	18.99	18.80	18.57	18.49	18.21	18.13	18.10	18.13	18.00	18.00	17.77	17.78	17.83
	0.100	0.013	0.013	0.011	0.015	0.008	0.007	0.020	0.015	0.018	0.017	0.029	0.041
Is40165	19.09	18.63	18.46	18.30	18.05	18.02	17.97	17.93	17.83	17.81	17.73	17.64	17.65
	0.095	0.012	0.011	0.012	0.011	0.013	0.007	0.015	0.012	0.016	0.019	0.031	0.047
Is40181	20.11	19.56	19.29	19.13	18.67	18.57	18.42	18.35	18.20	18.08	17.92	17.84	18.02
	0.245	0.024	0.016	0.018	0.020	0.012	0.008	0.024	0.014	0.022	0.019	0.028	0.062
Is50225	19.23	19.16	18.85	18.63	18.31	18.37	18.33	18.12	18.07	18.04	17.92	17.82	18.06
	0.135	0.022	0.024	0.016	0.019	0.022	0.018	0.025	0.018	0.024	0.030	0.034	0.063
Is50233	19.47	19.65	19.30	19.16	18.92	18.93	18.91	18.66	18.63	18.73	18.62	18.39	18.60
	0.151	0.078	0.065	0.070	0.060	0.074	0.066	0.065	0.075	0.069	0.093	0.110	0.190
Is50286	…	21.36	20.64	20.37	19.99	20.06	20.16	19.71	19.72	19.75	19.66	19.77	19.83
	…	0.296	0.199	0.144	0.108	0.117	0.137	0.139	0.140	0.155	0.168	0.249	0.261
Id50357	…	20.57	20.00	19.49	19.28	19.23	19.05	18.84	18.71	18.55	18.45	18.28	18.39
	…	0.063	0.033	0.025	0.031	0.023	0.016	0.037	0.024	0.036	0.032	0.044	0.070
Id50401	20.74	20.62	20.32	20.17	19.70	19.69	19.69	19.45	19.28	19.19	19.19	18.80	18.96
	0.539	0.116	0.096	0.095	0.096	0.099	0.099	0.137	0.105	0.104	0.152	0.096	0.195
Id50415	21.28	19.82	19.43	19.14	19.02	18.93	18.92	18.39	18.47	18.52	18.31	18.10	18.00
	1.172	0.100	0.105	0.084	0.099	0.092	0.080	0.074	0.073	0.090	0.101	0.067	0.109
Id50552	20.05	19.91	19.55	19.47	19.05	18.98	18.83	18.71	18.48	18.47	18.39	18.10	18.00
	0.243	0.127	0.125	0.116	0.089	0.092	0.106	0.113	0.081	0.094	0.102	0.095	0.093
Is50696	18.88	18.70	18.43	18.26	17.99	18.01	17.89	17.71	17.55	17.51	17.45	17.25	17.41
	0.122	0.054	0.044	0.036	0.026	0.024	0.036	0.045	0.050	0.049	0.059	0.059	0.098
Id50785	19.27	19.62	19.36	19.13	18.84	18.75	18.67	18.46	18.26	18.31	18.18	17.85	18.03
	0.131	0.125	0.133	0.095	0.085	0.080	0.093	0.080	0.067	0.083	0.082	0.071	0.094
Id50826	20.48	20.61	20.45	20.21	19.79	19.89	19.59	19.44	19.15	19.12	18.81	18.71	19.01
	0.512	0.233	0.213	0.191	0.145	0.183	0.125	0.154	0.116	0.124	0.115	0.114	0.268
Is50861	19.99	19.49	19.37	19.04	18.94	18.95	19.06	18.70	18.63	18.53	18.66	18.47	18.21
	0.335	0.179	0.186	0.143	0.140	0.168	0.190	0.172	0.155	0.139	0.188	0.177	0.180
Is50886	18.66	18.69	18.36	18.17	17.85	17.81	17.70	17.53	17.35	17.30	17.13	17.01	16.98
	0.153	0.129	0.102	0.079	0.056	0.060	0.047	0.050	0.036	0.032	0.031	0.026	0.050
Id50960	19.47	19.14	18.85	18.63	18.35	18.33	18.22	18.09	17.98	17.89	17.75	17.59	17.61
	0.144	0.031	0.033	0.027	0.026	0.029	0.025	0.035	0.031	0.034	0.033	0.041	0.064
Is51027	20.19	19.71	19.47	19.38	19.13	19.14	19.12	19.09	19.00	18.90	18.86	18.50	18.55
	0.268	0.037	0.027	0.024	0.036	0.027	0.022	0.048	0.043	0.054	0.038	0.069	0.093
Id70319	…	20.95	20.66	20.54	20.26	20.12	19.95	20.06	19.73	19.58	19.51	19.25	19.36
	…	0.105	0.068	0.061	0.078	0.069	0.032	0.097	0.044	0.086	0.060	0.109	0.200
Id70349	20.78	20.74	20.48	20.42	19.93	19.75	19.70	19.61	19.36	19.40	19.32	19.30	19.00
	0.394	0.091	0.049	0.048	0.060	0.048	0.023	0.070	0.039	0.070	0.063	0.104	0.144
Is80172	19.93	19.71	19.31	19.10	18.74	18.79	18.79	18.50	18.42	18.48	18.50	18.24	18.22
	0.206	0.033	0.021	0.017	0.022	0.015	0.010	0.025	0.024	0.033	0.026	0.045	0.109
SBKHP1	19.58	19.38	18.92	18.66	18.36	18.33	18.20	17.98	17.77	17.74	17.66	17.35	17.41
	0.194	0.121	0.107	0.091	0.085	0.096	0.089	0.107	0.085	0.093	0.098	0.078	0.115
SBKHP2	19.98	19.67	19.38	19.03	18.80	18.91	18.76	18.45	18.46	18.39	18.29	18.08	18.06
	0.359	0.317	0.348	0.262	0.259	0.345	0.325	0.333	0.336	0.342	0.352	0.338	0.421
SBKHP3	19.09	18.99	18.65	18.43	18.09	18.15	18.05	17.82	17.61	17.61	17.49	17.22	17.26
	0.202	0.221	0.216	0.192	0.170	0.226	0.197	0.226	0.179	0.201	0.197	0.167	0.226
SBKHP4	20.34	19.78	19.49	19.34	19.07	18.93	18.81	18.47	18.58	18.44	18.22	18.14	17.61
	0.463	0.405	0.414	0.414	0.388	0.429	0.400	0.404	0.453	0.437	0.417	0.429	0.325
SBKHP5	19.57	19.26	18.90	18.65	18.38	18.42	18.31	18.04	17.96	17.80	17.85	17.60	17.67
	0.227	0.113	0.119	0.111	0.118	0.156	0.158	0.179	0.161	0.156	0.195	0.173	0.217
SBKHP6	19.08	19.08	18.76	18.58	18.25	18.22	18.15	17.89	17.89	17.71	17.74	17.47	17.56
	0.169	0.254	0.267	0.262	0.252	0.292	0.294	0.334	0.331	0.310	0.360	0.336	0.483
SBKHP8	18.74	18.38	18.11	17.84	17.55	17.47	17.42	17.16	17.06	17.03	16.95	16.87	16.93
	0.110	0.077	0.073	0.091	0.105	0.128	0.131	0.144	0.133	0.145	0.156	0.171	0.234
SBKHP9	19.91	19.12	18.82	18.64	18.55	18.38	18.29	18.08	18.09	18.02	17.90	17.89	18.01
	0.342	0.152	0.165	0.165	0.186	0.214	0.210	0.251	0.256	0.276	0.285	0.329	0.459
SBKHP11	19.25	19.56	19.21	19.08	18.82	18.76	18.69	18.55	18.35	18.28	18.44	18.38	17.94
	0.144	0.179	0.182	0.179	0.190	0.217	0.207	0.274	0.234	0.239	0.337	0.366	0.308

TABLE 2 (*Continued*)

Name (1)	BATC03 (4210 Å) (1)	BATC04 (4546 Å) (1)	BATC05 (4872 Å) (1)	BATC06 (5250 Å) (1)	BATC07 (5785 Å) (1)	BATC08 (6075 Å) (1)	BATC09 (6710 Å) (1)	BATC10 (7010 Å) (1)	BATC11 (7530 Å) (1)	BATC12 (8000 Å) (1)	BATC13 (8510 Å) (1)	BATC14 (9170 Å) (1)	BATC15 (9720 Å) (1)
SBKHP12	19.81	19.37	19.11	18.85	18.60	18.59	18.46	18.30	18.16	18.13	18.00	17.90	18.01
	0.217	0.138	0.155	0.141	0.149	0.187	0.181	0.234	0.190	0.203	0.216	0.220	0.319
SBKHP13	19.73	19.68	19.34	19.14	18.90	18.95	18.80	18.68	18.59	18.44	18.36	18.12	18.23
	0.213	0.043	0.049	0.040	0.040	0.046	0.046	0.052	0.044	0.046	0.069	0.053	0.086
SBKHP14	20.08	19.52	19.40	19.09	18.91	18.79	18.84	18.64	18.53	18.62	18.40	18.35	18.60
	0.336	0.194	0.207	0.173	0.174	0.189	0.210	0.241	0.204	0.257	0.242	0.265	0.415
SBKHP15	19.73	19.32	18.99	18.74	18.45	18.49	18.40	18.17	18.08	17.92	17.85	17.66	17.84
	0.186	0.065	0.064	0.054	0.047	0.054	0.052	0.064	0.052	0.056	0.065	0.060	0.089
SBKHP16	…	19.93	19.63	19.48	19.43	19.47	19.13	19.41	19.05	19.36	19.21	19.78	19.76
	…	0.179	0.186	0.106	0.195	0.248	0.128	0.333	0.154	0.363	0.343	0.712	0.838
CFT5	20.09	20.74	20.44	20.00	19.33	19.49	19.30	19.02	18.78	18.62	18.59	18.29	18.15
	0.280	0.094	0.062	0.051	0.050	0.037	0.024	0.062	0.042	0.052	0.062	0.056	0.089
CFT6	21.15	20.97	20.47	20.36	20.07	20.05	19.80	19.85	19.66	19.68	19.65	19.23	19.97
	0.768	0.167	0.146	0.138	0.129	0.161	0.149	0.193	0.156	0.180	0.220	0.170	0.527
CFT37	20.79	20.32	19.69	19.71	19.51	19.05	18.94	19.10	18.67	18.93	18.38	18.15	18.79
	0.644	0.334	0.266	0.277	0.274	0.207	0.181	0.313	0.191	0.329	0.142	0.179	0.501
CFT38	20.32	19.99	19.86	19.57	19.22	19.25	19.06	18.58	18.52	18.43	18.33	18.33	18.16
	0.434	0.312	0.400	0.352	0.341	0.462	0.436	0.412	0.394	0.400	0.441	0.518	0.541
CFT39	19.37	19.75	19.52	19.20	18.76	18.76	18.64	18.35	18.23	18.12	18.11	17.75	18.01
	0.133	0.102	0.087	0.096	0.097	0.120	0.118	0.139	0.122	0.127	0.129	0.129	0.242
CFT41	…	20.57	19.96	19.65	19.24	19.02	18.77	19.20	19.04	18.88	18.87	19.11	19.38
	…	0.314	0.254	0.137	0.192	0.124	0.128	0.381	0.327	0.310	0.394	0.525	0.901
CFT97	20.95	20.16	19.97	19.70	19.64	19.62	19.41	19.30	19.48	19.50	19.56	19.15	19.14
	0.542	0.200	0.181	0.149	0.159	0.207	0.182	0.205	0.221	0.256	0.316	0.252	0.290
CFT113	22.59	20.94	20.51	20.41	20.03	20.12	19.95	19.58	19.48	19.46	19.38	19.17	19.38
	2.517	0.147	0.140	0.111	0.102	0.134	0.101	0.140	0.115	0.117	0.110	0.145	0.280

NOTE.—Central wavelength for each BATC filter (Å). Errors are given below each value.

obtained for Is50286, Id50357, Id70319, SBKHP16, and CFT41, owing to low S/Ns. Because of the low angular resolution, and given the Schmidt pixel size of 1.″7, the different sizes of different clusters are not evident in our CCD images.

2.4. Comparison with Previous Photometry

Zhou et al. (2003) presented the relationships between the BATC intermediate-band system and the *UBVRI* broadband system, using the standard-star catalogs of Landolt (1983, 1992) and Galadí-Enríquez et al. (2000). The coefficients of two relationships are

$$m_B = m_{04} + 0.2201(m_{03} - m_{05}) + 0.1278 \pm 0.076 \quad (4)$$

and

$$m_V = m_{07} + 0.3292(m_{06} - m_{08}) + 0.0476 \pm 0.027. \quad (5)$$

Using equations (4) and (5), we transformed the magnitudes of 42 GCs in the BATC03, BATC04, and BATC05 bands to their *B*-band equivalents, and from BATC06, BATC07, and BATC08 bands to those in the *V* band. Figure 1 plots the comparison of *V* (BATC) and $(B - V)$ (BATC) photometry with previously published measurements of Perelmuter & Racine (1995) and Chandar et al. (2001). In this figure, our magnitudes/colors are on the *x*-axis, and the difference between our magnitudes/colors and those of Perelmuter & Racine (1995) and Chandar et al. (2001) are on the *y*-axis. Table 3 lists data used in this comparison. The mean *V* magnitude and color differences (in the sense of this paper minus Perelmuter & Racine [1995] and Chandar et al. [2001]) are $\langle \Delta V \rangle = -0.116 \pm 0.028$ and $\langle \Delta(B - V) \rangle = -0.017 \pm 0.027$, respectively. The uncertainties in $\langle \Delta V \rangle$ and $\langle \Delta(B - V) \rangle$ are, respectively,

$$\sqrt{[\Sigma(\langle \Delta V \rangle - \overline{\langle \Delta V \rangle})^2] / [N(N-1)]} \quad (6)$$

and

$$\sqrt{[\Sigma(\langle \Delta(B-V) \rangle - \overline{\langle \Delta(B-V) \rangle})^2] / [N(N-1)]}. \quad (7)$$

Uncertainties in *B* (BATC) and *V* (BATC) have been added linearly [i.e., $\sigma_B = \sigma_{\rm BATC04} + 0.2201(\sigma_{\rm BATC03} + \sigma_{\rm BATC05})$ and $\sigma_V = \sigma_{\rm BATC07} + 0.3292(\sigma_{\rm BATC06} + \sigma_{\rm BATC08})$] to reflect the errors in the three filter measurements. For the colors, we add the errors in quadrature; i.e., $\sigma_{(B-V)} = (\sigma_B 2 + \sigma_V 2)^{1/2}$. From Figure 1 and Table 3, it can be seen that there is good agreement in the photometric measurements.

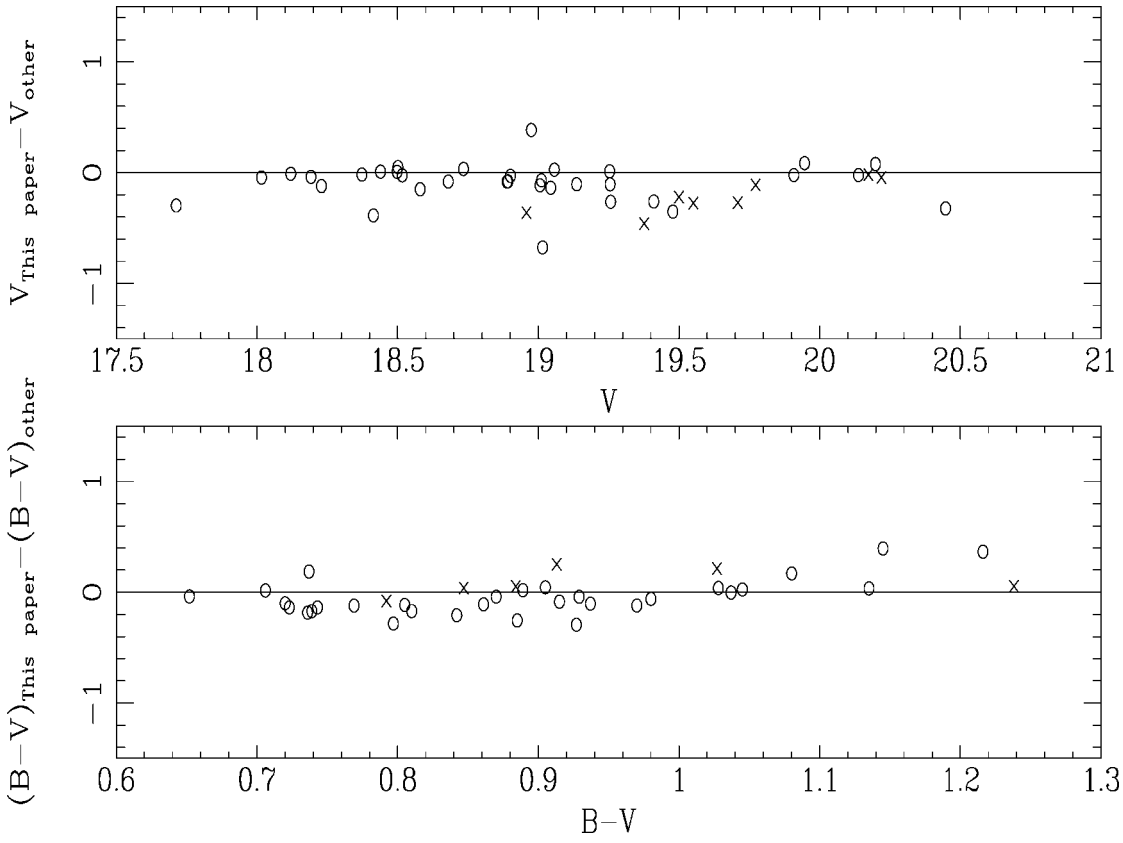

FIG. 1.—Comparison of cluster photometry with previous measurements by Perelmuter & Racine (1995; *open circles*) and Chandar et al. (2001; *crosses*).

2.5. Reddening

In order to obtain intrinsic SEDs for the sample GCs, the photometric data are corrected for reddening from the foreground extinction contribution of the Milky Way, and for internal reddening due to varying optical paths through the disk of M81. The total reddening determination for the M81 field (the foreground plus M81 contribution) has been measured by a number of authors (e.g., Freedman et al. 1994; Kong et al. 2000). We only mention here that Kong et al. (2000) obtained the reddening maps of the M81 field based on the images observed by the BATC Multicolor Sky Survey in the 13 intermediate-band filters from 3800 to 10000 Å. To determine the metallicity, age, and reddening distributions for the M81 field, Kong et al. (2000) found the best match between the observed colors and the predictions from single stellar population models of G. Bruzual & S. Charlot (1996, unpublished; hereafter BC96). A map of the interstellar reddening in a substantial portion of M81 was obtained. For a few clusters that fall near the edges of the images, Kong et al. (2000) did not obtain reddening values. For these clusters we adopt a mean reddening value of 0.13, as did Chandar et al. (2001). The local reddening values for these GCs are listed in column (4) of Table 1 in Ma et al. (2005). Figure 2 plots the intrinsic SEDs of 42 GCs (relative to the flux of filter BATC08) in the 13 BATC intermediate-band filters.

2.6. Analysis of the SEDs of the GCs

Schroder et al. (2002) observed moderate-resolution spectroscopy of 16 M81 GCs using the Low-Resolution Imaging Spectrograph on the Keck I Telescope. By comparing the observed age-sensitive index Hβ against Mg2 and isochrones from the evolutionary synthesis models from Worthey (1994) and Fritze-v. Alvensleben & Burkert (1995), Schroder et al. (2002) find that SBKHP15[3] is younger than the other GCs. As we know, a lower metallicity and younger age can cause the fluxes in longer filter bands to be lower. The metallicity of this cluster is nearly the same as that of SBKHP8. So from the SEDs of Figure 2, we can conclude that SBKHP16 is younger than SBKHP8, as its SED is lower than those of SBKHP8 in

[3] In fact, SBKHP15 should be SBKHP16. We referred the Table 6 of Perelmuter & Racine (1995) and found that the R.A. and decl. of ID 50867 are $09^h55^m40\overset{s}{.}194$ and $69°07'30\overset{''}{.}82$ (J2000.0), respectively, and the R.A. and decl. of ID 50889 are $09^h55^m51\overset{s}{.}995$ and $69°07'39\overset{''}{.}32$ (J2000.0), respectively; i.e., the R.A. and decl. of SBKHP15 and 16 should be exchanged in Schroder et al. (2002).

TABLE 2
COMPARISON OF PHOTOMETRY WITH PREVIOUS MEASUREMENTS

	V		$B-V$	
NAME	Previous Work	BATC	Previous Work	BATC
Is40083	18.39	18.373 ± 0.021	0.69	0.652 ± 0.043
Is40165	18.23	18.192 ± 0.019	0.69	0.706 ± 0.040
Is40181	18.93	18.901 ± 0.030	1.09	0.970 ± 0.087
Is50225	18.43	18.439 ± 0.032	0.97	0.929 ± 0.065
Is50233	19.18	19.044 ± 0.107	0.89	0.769 ± 0.165
Is50286	20.16	20.138 ± 0.194	0.89	…
Id50357	19.67	19.410 ± 0.047	1.27	…
Id50401	19.93	19.908 ± 0.160	1.22	0.927 ± 0.302
Id50415	19.24	19.136 ± 0.157	0.85	1.216 ± 0.412
Id50552	19.52	19.257 ± 0.157	1.14	0.885 ± 0.261
Is50696	18.13	18.120 ± 0.046	0.92	0.805 ± 0.101
Id50785	19.08	19.011 ± 0.143	0.86	0.723 ± 0.232
Id50826	19.86	19.946 ± 0.268	1.08	0.797 ± 0.475
Is50861	19.69	19.015 ± 0.242	0.88	0.743 ± 0.381
Is50886	18.06	18.016 ± 0.102	0.91	0.870 ± 0.211
Id50960	18.49	18.498 ± 0.044	0.86	0.905 ± 0.083
Is51027	19.36	19.255 ± 0.053	0.55	0.737 ± 0.115
Id70319	20.77	20.447 ± 0.121	0.99	…
Id70349	20.12	20.198 ± 0.092	0.91	0.739 ± 0.210
Is80172	18.97	18.892 ± 0.033	0.91	1.080 ± 0.089
SBKHP1	18.54	18.516 ± 0.147	1.10	1.135 ± 0.238
SBKHP2	18.97	18.889 ± 0.459	1.02	1.045 ± 0.659
SBKHP3	18.35	18.229 ± 0.308	1.04	0.980 ± 0.439
SBKHP4	19.24	19.253 ± 0.666	1.05	0.842 ± 0.895
SBKHP5	18.45	18.501 ± 0.206	1.04	1.037 ± 0.280
SBKHP6	18.80	18.414 ± 0.434	0.97	0.861 ± 0.558
SBKHP8	18.01	17.713 ± 0.177	1.04	0.937 ± 0.212
SBKHP9	18.76	18.680 ± 0.311	0.98	0.810 ± 0.407
SBKHP11	18.59	18.975 ± 0.320	0.82	0.720 ± 0.407
SBKHP12	18.70	18.734 ± 0.257	1.00	0.915 ± 0.338
SBKHP13	19.12	19.006 ± 0.068	0.87	0.889 ± 0.122
SBKHP14	19.03	19.057 ± 0.293	0.92	0.736 ± 0.429
SBKHP15	18.73	18.580 ± 0.083	0.99	1.028 ± 0.146
SBKHP16	19.83	19.478 ± 0.312	0.75	1.145 ± 0.799
CFT5	19.826 ± 0.008	19.551 ± 0.079	1.184 ± 0.029	1.238 ± 0.187
CFT6	20.263 ± 0.010	20.219 ± 0.227	0.813 ± 0.035	1.027 ± 0.433
CFT37	19.882 ± 0.009	19.772 ± 0.433	0.661 ± 0.013	0.913 ± 0.688
CFT38	19.835 ± 0.006	19.376 ± 0.609	0.808 ± 0.012	0.847 ± 0.785
CFT39	19.319 ± 0.005	18.958 ± 0.168	0.832 ± 0.009	0.884 ± 0.226
CFT41	19.721 ± 0.006	19.500 ± 0.278	0.696 ± 0.009	…
CFT97	19.980 ± 0.008	19.709 ± 0.276	0.870 ± 0.023	0.792 ± 0.453
CFT113	20.192 ± 0.014	20.173 ± 0.183	1.065 ± 0.058	1.355 ± 0.754

longer filter bands. In particular, SBKHP16 has very low fluxes in the BATC14 and BATC15 filter bands. We compare its SEDs with those of SBKHP8 and find that the intrinsic flux (relative to the flux of the BATC08 filter band) is 1.607 versus 0.641 in the BATC14 filter band, and 1.505 versus 0.649 in the BATC15 filter band, nearly 2.5 times greater.

2.7. Ages

A single GC is a stellar population with a single age and chemical abundance. Globular clusters are ideal systems for characterization with simple stellar population (SSP) models.

BC96 models are given for SSPs of metallicities $Z = 0.0004$, 0.004, 0.008, 0.02, 0.05, and 0.1. These models are based on the Padova group evolutionary tracks (Bressan et al. 1993; Fagotto et al. 1994; Girardi et al. 1996), which use the radiative opacities of Iglesias et al. (1992), together with a helium abundance $Y = 2.5Z + 0.23$ (the reference solar metallicity is $Z_{\odot} = 0.02$). BC96 models further use the Lejeune et al. (1997) standard-star library. The ages in the BC96 models range from 0 to 20 Gyr. A Salpeter (1955) initial mass function of $\Phi(M) = AM^{-\alpha}$, with $\alpha = 2.35$, is used with a normalization constant $A = 1$, a lower cutoff mass $M_{\rm l} = 0.1\ M_{\odot}$, and an upper cutoff mass $M_u = 125\ M_{\odot}$.

To proceed with the comparisons, we first convolve the SEDs

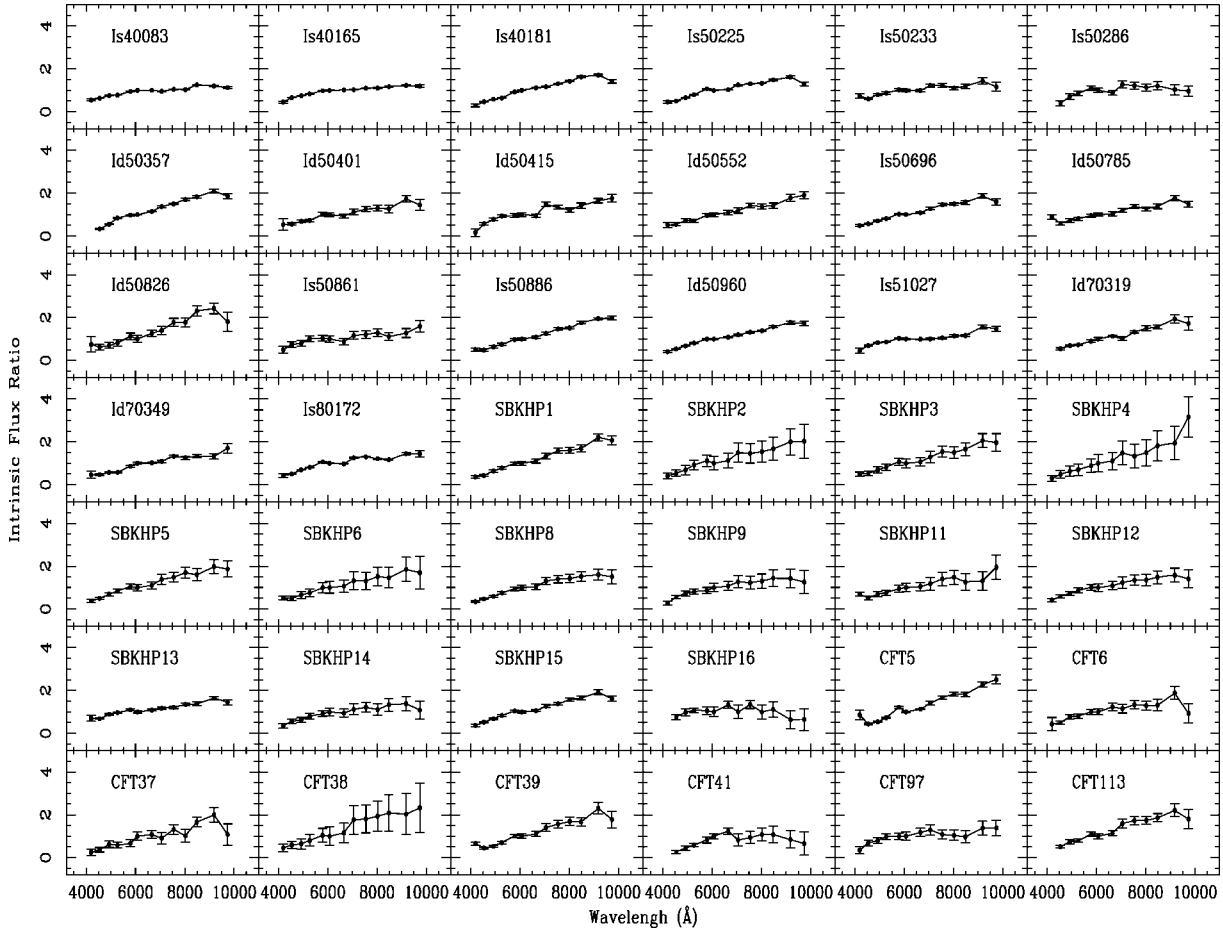

FIG. 2.—Intrinsic spectrophotometric energy distributions for 42 GCs in M81.

of the BC96 models with the BATC filter profiles to obtain the optical and near-infrared integrated luminosities. The integrated luminosities $L_{\lambda_i}(t, Z)$ of the ith BATC filter can be calculated as

$$L_{\lambda_i}(t, Z) = \frac{\int F_\lambda(t, Z)\varphi_i(\lambda)\, d\lambda}{\int \varphi_i(\lambda)\, d\lambda}, \qquad (8)$$

where $F_\lambda(t, Z)$ is the SED at age t in metallicity Z, and $\varphi_i(\lambda)$ is the response function of the ith filter of the BATC filter system ($i = 3, 4, \ldots, 15$). All integrated colors of the BC96 models are calculated relative to the BATC08 filter band ($\lambda = 6075$ Å):

$$C_{\lambda_i}(t, Z) = L_{\lambda_i}(t, Z)/L_{6075}(t, Z). \qquad (9)$$

From this equation, we can obtain model intermediate-band colors for SSP models with different metallicities.

In order to study the stellar populations of these GCs, we use the five ages 1, 2, 3, 8, and 16 Gyr of the BC96 SSP models for two metallicities: a metal-poor model of $Z = 0.0004$, and a more metal-rich model of $Z = 0.004$. The best SED fit between a globular cluster and the SSP models is found by minimizing the color differences between intrinsic integrated color of a cluster and the integrated color of the models:

$$R^2(n, t, Z) = \frac{\sum_{i=3}^{15} [C_{\lambda_i}^{\rm intr}(n) - C_{\lambda_i}^{\rm SSP}(t, Z)]^2/\sigma_i^2}{\sum_{i=3}^{15} 1/\sigma_i^2}, \qquad (10)$$

where $C_{\lambda_i}^{\rm SSP}(t, Z)$ represents the integrated color in the ith filter of an SSP at age t in a metallicity Z model, and $C_{\lambda_i}^{\rm intr}(n)$ is the intrinsic integrated color for a cluster. The differences are weighted by $1/\sigma_i^2$, where σ_i is the observational uncertainty of the passbands. Figure 3 shows the results of SED fits; the filled circle represents the intrinsic integrated color of a cluster, and the thick line represents the best fit of the integrated color of an SSP model.

From Figure 3, we can see that of these 42 M81 GCs, there are 11 for which our estimates give ages younger than 8 Gyr. The results tell us that M81 includes a population of intermediate-age GCs with ages of a few Gyr. Similar clusters have

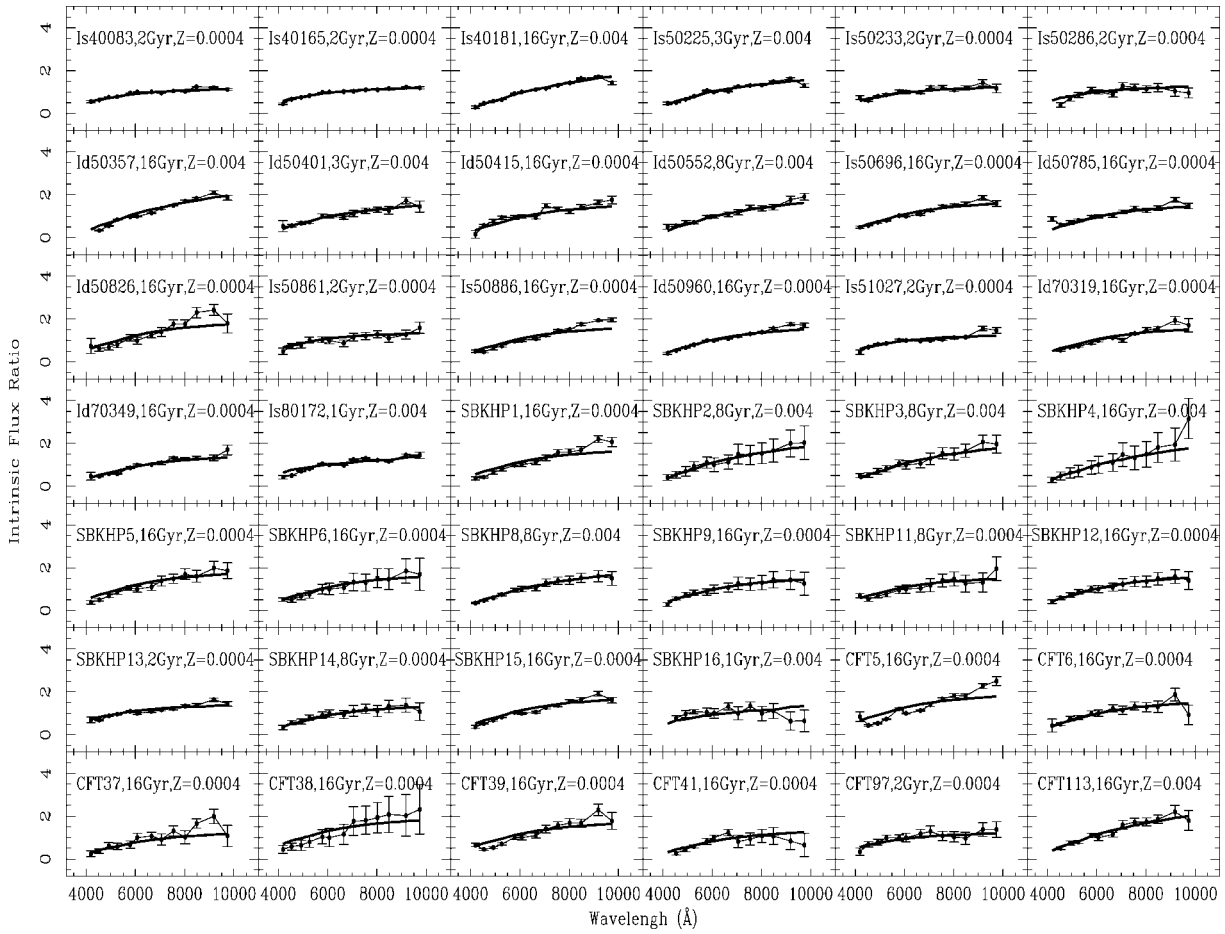

FIG. 3.—Map of the fit of the integrated color of an SSP model to intrinsic integrated color for sample GCs. Filled circles represent the intrinsic integrated color of a GC, and the thick lines represent the best fit of the integrated color of an SSP model.

been observed in both M31 and M33 (Brodie & Huchra 1990, 1991; Jiang et al. 2003; Beasley et al. 2004; Burstein et al. 2004; Puzia et al. 2005; Sarajedini et al. 1998, 2000; Ma et al. 2002). For SBKHP16, Schroder et al. (2002) derived an age between 1.5 and 3 Gyr, and our result is consistent with this estimate, giving an age of between 1 and 2 Gyr. Our results also show that the age of SBKHP13 is between 2 and 3 Gyr, which was not given by Schroder et al. (2002), because the value of the index Hβ was not derived in that paper. The ages of the other GCs given by Schroder et al. (2002) that are obtained in this paper are also fully consistent with those results.

3. SUMMARY

We have obtained SEDs of 42 M81 GCs in 13 intermediate-band filters with the BATC 0.6/0.9 m Schmidt telescope. The BATC filter system is specifically designed to exclude most of the bright and variable night-sky emission lines, including the OH forest, and it can present accurate SEDs of objects observed. This paper confirms the conclusions of Schroder et al. (2002), that M81 contains clusters as young as a few Gyr. Such young GCs have also been observed in both M31 and M33 (Brodie & Huchra 1990, 1991; Jiang et al. 2003; Beasley et al. 2004; Burstein et al. 2004; Puzia et al. 2005; Sarajedini et al. 1998, 2000; Ma et al. 2002).

We would like to thank the anonymous referee for his/her insightful comments and suggestions, greatly improved this paper. This work has been supported by the Chinese National Science Foundation (No. 10473012) and by the Chinese National Key Basic Research Science Foundation (NKBRSF TG199075402).

REFERENCES

Beasley, M., et al. 2004, AJ, 128, 1623
———. 2005, AJ, 129, 1412
Bressan, A., et al. 1993, A&AS, 100, 647
Brodie, J. P., & Huchra, J. P. 1990, ApJ, 362, 503
———. 1991, ApJ, 379, 157
Burstein, D., et al. 2004, ApJ, 614, 158
Chandar, R., Ford, H. C., & Tsvetanov, Z. 2001, AJ, 122, 1330
Fagotto, F., Bressan, A., Bertelli, G., & Chiosi, C. 1994, A&AS, 105, 39
Fan, X., et al. 1996, AJ, 112, 628
Freedman, W. L., Wilson, C. D., & Madore, B. F. 1994, ApJ, 427, 628
Fritze-v. Alvensleben, U., & Burkert, A. 1995, A&A, 300, 58
Fukugita, M., et al. 1996, AJ, 111, 1748
Galadí-Enríquez, D., Trullols, E., & Jordi, C. 2000, A&AS, 146, 169
Girardi, L., Bressan, A., Chiosi, C., Bertelli, G., & Nasi, E. 1996, A&AS, 117, 113
Iglesias, C. A., Rogers, F. J., & Wilson, B. G. 1992, ApJ, 397, 717
Jiang, L. H., Ma, J., Zhou X., Chen, J. S., Wu, H., & Jiang, Z. J. 2003, AJ, 125, 727
Kong, X., et al. 2000, AJ, 119, 2745
Landolt, A. U. 1983, AJ, 88, 439
———. 1992, AJ, 104, 340
Lejeune, Th., Cuisinier, F., & Buser, R. 1997, A&AS, 125, 229
Ma, J., Zhou, X., Chen, J., Wu, H., Jiang, Z., Xue, S., & Zhu, J. 2002, A&A, 385, 404
Ma, J., et al. 2005, PASP, 117, 256
Oke, J. B., & Gunn, J. E. 1983, ApJ, 266, 713
Perelmuter, J. M., Brodie, J. P., & Huchra, J. 1995, AJ, 110, 620
Perelmuter, J. M., & Racine, R. 1995, AJ, 109, 1055
Puzia, T. H., Perrett, K. M., & Bridges, T. J. 2005, A&A, 434, 909
Sarajedini, A. A., Geisler, D., Harding, P., & Schommer, R. 1998, ApJ, 508, L37
Sarajedini, A. A., Geisler, D., Schommer, R., & Harding, P. 2000, AJ, 120, 2437
Salpeter, E. E. 1955, ApJ, 121, 161
Schroder, L. L., Brodie, J. P., Kissler-Patig, M., Huchra, J. P., & Phillips, A. C. 2002, AJ, 123, 2473
Stetson, P. B. 1987, PASP, 99, 191
Worthey, G. 1994, ApJS, 95, 107
Wu, H., et al. 2002, AJ, 123, 1364
Yan, H. J., et al. 2000, PASP, 112, 691
Zheng, Z. Y., et al. 1999, AJ, 117, 2757
Zhou, X., Jiang, Z. J., Xue, S. J., Wu, H., Ma, J., & Chen, J. S. 2001, Chinese J. Astron. Astrophys., 1, 372
Zhou, X., et al. 2003, A&A, 397, 361
———. 2004, AJ, 127, 3642